Laser-based microfocused x-ray source for mammography: Feasibility study

A. Krol
SUNY Health Science Center, Department of Radiology, 750 E. Adams St., Syracuse, New York 13210

A. Ikhlef and J. C. Kieffer
INRS-Énergie et Matériaux, Université du Québec, Varennes, Québec, 1650 Montée Sainte-Julie, J3X 1S2, Canada

D. A. Bassano
SUNY Health Science Center, Department of Radiation Therapy, 750 E. Adams St., Syracuse, New York 13210

C. C. Chamberlain
SUNY Health Science Center, Department of Radiology, 750 E. Adams St., Syracuse, New York 13210

Z. Jiang and H. Pépin
INRS-Energie et Matériaux, Université du Québec, Varennes, Québec, 1650 Montée Sainte-Julie, J3X 1S2, Canada

S. C. Prasad
SUNY Health Science Center, Department of Radiation Therapy, 750 E. Adams St., Syracuse, New York 13210

(Received 10 July 1996; accepted for publication 4 March 1997)

A laser-produced plasma (LPP) x-ray source with possible application in mammography was created by focusing a laser beam on a Mo target. A Table-Top-Terawatt (TTT) laser operating at 1 J energy per pulse was employed. A dual pulse technique was used. Maximum energy transfer ($\sim$10%) from laser light to hot electrons was reached at a 150 ps delay between pulses and the conversion efficiency (hard x-ray yield/laser energy input) was $\sim 2\times 10^{-4}$. The created LPP x-ray source is characterized by a very small focal spot size (tens of μm), Gaussian brightness distribution, and a very short pulse duration (a few ps). The spectral distribution of the generated x rays was measured. Images of the focal spot, using a pinhole camera, and images of a resolution pattern and a mammographic phantom were obtained. The LPP focal spot modulation transfer function for different magnification factors was calculated. We have shown that the LPP source in conjunction with a spherically bent, high throughput, crystal monochromator in a fixed-exit Rowland circle configuration can be used to create a narrow band tunable mammography system. Tunability to a specific patient breast tissue thickness and density would allow one to significantly improve contrast and resolution (exceeding 20 lp/mm) while lowering the exposure up to 50% for thicker breasts. The prospects for the LPP x-ray source for mammographic application are discussed. [S0094-2405(97)02305-5]

Key words: mammography, laser-based x-ray source, x-ray spectra

I. INTRODUCTION

The electron-impact x-ray tube, pioneered 100 yrs ago by Röntgen, has reached its technological limit, and after many years of improvements it is clear that some of the inherent deficiencies of this x-ray source for radiology cannot be overcome. These deficiencies are the heat-dissipation problem, which limits the density of the power that can be delivered by the electron beam, and the related problem of the limit on the minimum focal spot size. The relatively large focal spot size prevents effective work in a high magnification regime and limits the ability to detect small calcifications and structural characteristics of soft tissue masses, both of which are very important in the diagnosis of breast cancer.

A laser-driven, photon-impact x-ray source for mammography may be able to overcome these limitations. The x-ray source is created upon collision of a visible or infrared photon beam with the surfaces of solids. Presently, modern high-power lasers can deliver in excess of 10^{19} W/cm^2 to a target area as small as 5 μm in diameter. This should be contrasted with the power density delivered by traditional electron-impact x-ray tubes that typically does not exceed 10^9 W/cm^2. An extremely short x-ray pulse duration, determined by the laser pulse temporal structure, typically of the order of 10^{-12} s and a very small focal spot diameter, defined by the laser beam diameter on the target, are the inherent features of this new x-ray source.

The feasibility of the laser-based x-ray source for diagnostic radiology was recently investigated by Herrlin *et al.*[1] Polychromatic, incoherent, x rays (HVL=10 mm of Al) were generated by focusing a Table-Top-Terawatt (TTT) la-

ser light pulse (3×10^{17} W/cm^2) on a solid target made of tantalum foil.

The aim of the present work was to investigate applicability of the LPP x-ray source to mammography. We performed experimental and theoretical feasibility studies and considered the possible impact of the laser-driven x-ray source on future clinical mammography systems.

II. MATERIALS AND METHODS

A. Mechanism of x-ray generation from laser-produced plasma

Consider a laser pulse that strikes a solid target. If the power density delivered by the laser exceeds $\sim5\times10^{12}$ W/cm^2 vaporization and ionization of the target occurs.[2] As a result, with subpicosecond laser pulses, a near-solid density expanding thin layer of plasma with a rather steep density gradient is created. The ensuing density profile can be approximately described[2] by $n_e(z)\propto\exp(-zC/L)$, where $n_e(z)$ is the electron density at distance z from the surface, C is a constant, and L is the gradient scale length that changes during the plasma expansion. In our previous experiments,[2] utilizing a single pulse irradiation technique, we observed that the parameter L was smaller than the laser-light wavelength ($L<\lambda_{\text{laser}}$). Typically for $\lambda_{\text{laser}}=0.53$ μm at 5×10^{17} W/cm^2, the estimated value of L was 0.1 μm and the initial thickness of the dense plasma layer was ~0.2 μm electron temperature, T_e, was $\sim5\,00$ eV, and electron density was $n_e\approx6\times10^{22}$ cm^{-3}.[3] In this stage of the interaction, the laser light beam is in effect interacting with a thin, expanding layer of ionized matter of near-solid density. The expansion can be impeded by the light pressure, as observed by Liu and Umstadter[4] and confirmed in our experiments.[5] We note that the laser light with 10^{18} W/cm^2 intensity, has an electric field of the order of 3×10^{10} V/m and exerts a light pressure of 0.3 Gbar.[6] The characteristic time of temperature change of the dense plasma is comparable to the ultrashort (i.e., femtosecond time scale) laser pulse duration. The extent of the expansion is therefore set by the laser pulse duration. It is believed that for the laser pulse intensity in the 10^{16}–10^{18} W/cm^2 range, hot (suprathermal) electrons and very energetic ions are produced primarily by linear resonance absorption in p polarization.[7] The inverse bremsstrahlung and Raman instabilities might play some role in the energy transfer from laser radiation to hot electron as well.[3] As evidenced by our previous studies,[2] the temperature of suprathermal electrons is controlled by irradiation conditions following the empirical law $T_h\propto(I\lambda_{\text{laser}}{}^2)^{1/3}$. In the present experiments with Mo targets the temperature of hot electrons was estimated as $T_h\approx25$ keV, and we established that up to 10% of the laser energy was transferred to hot electrons. In order to intensify the energy transfer from laser light to hot electrons the gradient scale-length parameter L of the dense plasma layer has to be optimized during the laser light–solid target interaction. In our experiments this was accomplished by double-pulse irradiation. In this technique the first low-intensity pulse creates a preformed dense and cold plasma layer on the target surface. The second, high-intensity pulse is delayed by a preset time interval (0–200 ps) and interacts with the preformed plasma, allowing for more efficient energy transfer to hot electrons. It is possible because the characteristic parameter L of the dense plasma seen by the main pulse is controlled by the delay interval and can be optimized.

A majority of the hot electrons leave the dense-plasma region and consequently a very strong space-charge field is being set up at the target along with a low-density high-temperature plasma created above the target. Emission of electrons and ions with MeV energies from laser-produced plasma (LPP) was recently reported.[8,9] A significant fraction of hot electrons streams back toward the positively charged space-charge region on the target surface. As a result, the suprathermal electrons penetrate the target producing a burst of incoherent x rays, composed of continuous bremsstrahlung emission and discrete characteristic x-ray emission lines.[3] The peak power of the burst of x rays emitted by LPP sources exceeds that produced by a synchrotron light source. The duration of the LPP-generated x-ray burst is controlled by and is longer than the duration of the laser pulse and in our experiments it did not exceed 4 ps for 0.4 ps of the laser pulse duration.[3] The LPP x-ray source size gradually increases with time and its characteristic dimension is defined by the initial size of the laser focal spot and the laser pulse duration. The x-ray focal spot enlargement is caused by lateral transport occurring in the dense plasma layer, which leads to the lateral expansion of the plasma. In our experiments the full width at half-maximum (FWHM) of the LPP x-ray source brightness distribution was ~50 μm while the laser focal spot size was of the order of 10 μm. We have found that the conversion efficiency of the laser-driven x-ray source (F_x) defined as the ratio of the energy emitted in the x-ray burst produced by the laser-light pulse to the energy in the laser-light pulse, is approximately proportional to the square root of the laser beam intensity, i.e., to the peak electric field of the laser light and to the atomic number Z of the target, $F_x\propto E_{\text{peak}}Z$. Validity of this relation was also verified by Kmetec *et al.*[8] We note equivalency with the x-ray tube conversion efficiency law, $F_x\propto VZ$.[10] It should be emphasized that the LPP x-ray yield (i.e., the total energy emitted in x rays) strongly depends on the target surface structure and the irradiation conditions.

B. Experimental design

For the present feasibility studies, we used the existing compact and relatively high-energy system of the INRS laboratory in Varennes. The geometry utilized in this work is shown in Fig. 1. The INRS laser system consists of a TTT laser operating at 1000 mJ, 0.03 Hz repetition rate, generating infrared coherent radiation with 1 μ wavelength ($\lambda_{\text{laser}}=1.053$ μm) in 550 fs pulses. The initial laser beam is split by a Potassium Dihydrogen Phospate (KDP) crystal into two pulses: a primary, low-intensity, infrared pulse with unchanged frequency (400 mJ, $\lambda_{\text{laser}}=1.053$ μm, 550 fs) and a secondary, high-intensity, green light pulse with doubled frequency (400 mJ, $\lambda_{\text{laser}}=0.53$ μm, 400 fs). The delay be-

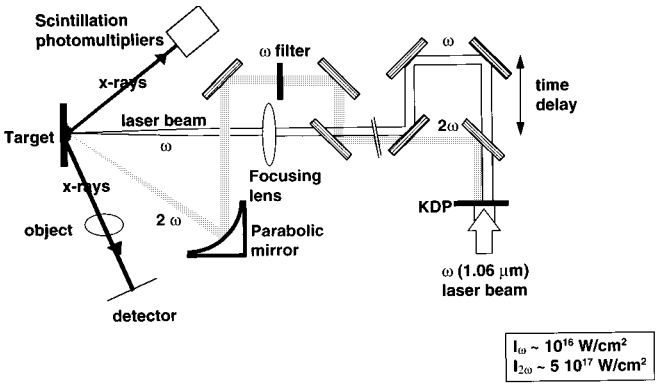

FIG. 1. The experimental geometry utilized in this work.

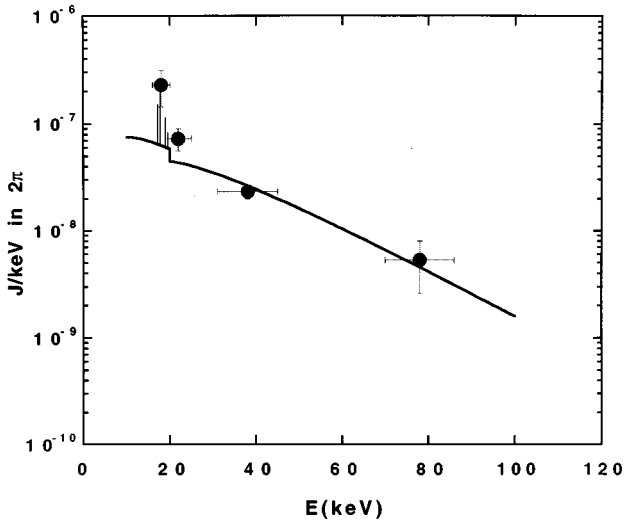

FIG. 2. X-ray energy emitted in 2π srd per 1 kev bandwidth of x rays (denoted as ''J/keV in 2π'' on the vertical axis). The solid circles represent the experimentally obtained spectral distribution of radiation generated in the present experiment with a high-intensity green beam alone (5×10^{17} W/cm^2, $\lambda_{laser} = 0.53$ μm, thick Mo target). The solid curve represents the theoretically calculated spectrum assuming 5% of laser energy transferred into hot electrons.

tween the two pulses can be varied from 0 to 200 ps. The primary infrared beam is focused by a lens ($f/6$) on a Mo target forming a controlled preplasma ~ 100 μm in diameter, while the secondary, delayed, green light beam is focused by means of an off-focal parabolic mirror ($f/3$) to a spot ~ 10 μm in diameter in the center of the preplasma layer. The specific beams diameters were selected in order to optimize the primary to the secondary pulse intensity ratio. The irradiation intensities were 10^{16} and 5×10^{17} W/cm^2 for the primary and the secondary pulses, respectively.

The target was kept in a vacuum chamber. A glass window allowed focusing the laser light pulses on the target while a 0.5 mm Al window was used to filter out soft (below 10 keV) x-ray component from the resulting x-ray spectrum.

X-ray yield was measured with a battery of several photomultipliers-NaI(TI) scintillator detectors each equipped with a different set of K-edge filters utilizing the Ross filter technique. In this device each detector has its maximum spectral sensitivity located in a different part of the investigated spectrum.[11] The absolute energy spectra (i.e., the number of emitted x-ray photons versus energy per x-ray photon energy interval) was obtained from deconvolution of the various photomultipliers signals using a weighted least-squared curve fitting procedure for the entire 10–100 keV interval investigated.[11] Background signals were eliminated by the use of very thick lead shielding and electron sweeping magnets in front of the detectors. The detector system was carefully calibrated to investigate conversion efficiency from laser light to x rays in the 10–100 keV range.[11]

The images of the focal spot were obtained using a pinhole camera and photographic film. The images of test objects were obtained using suitable filters and photographic film.

C. Experimental results

It can be shown that the energy distribution of the continuos spectra due to the LPP x-ray source can be well described by $\exp(-h\nu/T_h)$, where $h\nu$ is the x-ray energy and T_h is the temperature of hot electrons.[12] The temperature of suprathermal (hot) electrons created in the present experiment was estimated from the slope of the hard x-ray spectra (10–100 keV) to be at ~ 25 keV. The experimentally obtained spectral distribution of radiation generated in the present experiment by the high-intensity green light pulse ($\lambda_{laser} = 0.53$ μm) alone is shown in Fig. 2. We observe the Mo K_α emission line superimposed on a continuous spectrum with a mean energy of 25 keV. In the dual beam technique, the maximum conversion efficiency of about 2×10^{-4} was reached. We note that the conversion efficiency of an x-ray tube with a Mo target at $25\,kV_P$ can be estimated as 9×10^{-4}. The emitted x-ray flux at 20 keV within a 1 keV bandwidth per laser shot can be estimated as 7×10^9 photons in 2π srd.

The fraction of the laser energy transferred to hot electrons (F_{le}) was estimated using the characteristic Mo K_α emission;[12] the results are shown in Fig. 3 as a function of time delay (t_d) between the primary pulse forming preplasma and the secondary pulse. We observe a very significant increase in F_{le} with increasing time delay. A maximum was reached at the 150 ps delay. We conclude that at this specific time delay the L parameter of the preformed dense plasma reaches its optimal value for our experimental conditions.

The x-ray focal spot created by LPP was imaged using a pinhole camera and is shown in Fig. 4 along with an image of a microfocal spot created by a dedicated clinical Mo mammography unit. We observe that the characteristic dimension of the LPP focal spot is reduced by an order of magnitude as compared to the microfocal spot produced by an x-ray tube. The LPP x-ray spot can be best described by a two-dimensional Gaussian brightness distribution, as can be inferred from the analysis of an image of a resolution pattern shown in Fig. 5. In the analysis we followed the methodology described in Refs. 13 and 14. The edge spread function (ESF) inferred from the microdensitometer trace of the reso-

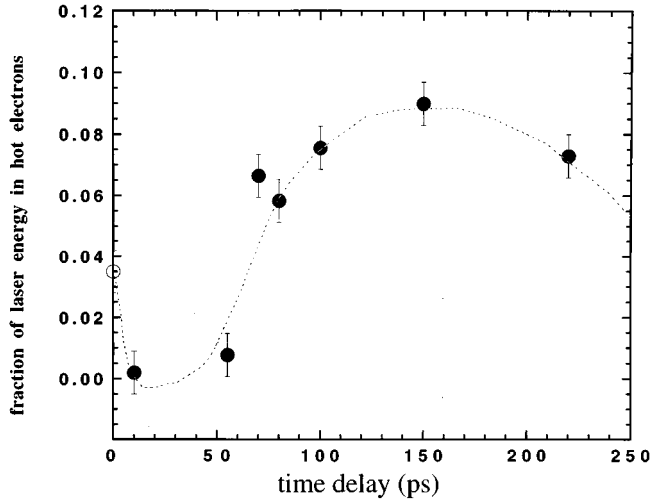

FIG. 3. The fraction of the laser energy transferred to hot electrons as a function of time delay obtained for a thick Mo target.

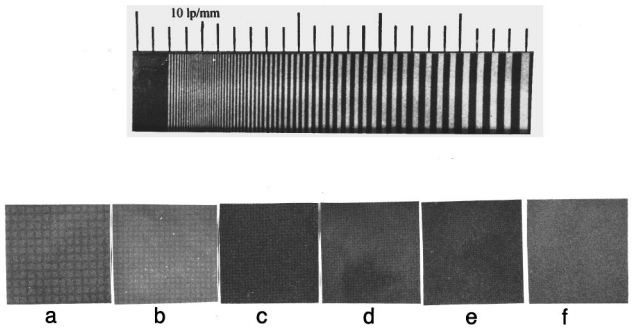

FIG. 5. Top: an image of a resolution pattern obtained at magnification two and a scale added with a large division equal to 1 cm. Bottom: images of stainless steel meshes in a Kodak ITO mammographic phantom obtained in magnification 1.05: (a) mesh #40, $d=0.46$ mm; (b) mesh #60, $d=0.28$ mm; (c) mesh #100, $d=0.168$ mm; (d) mesh #120, $d=0.141$ mm; (e) mesh #160, $d=0.104$ mm; (f) mesh #200, $d=0.089$ mm; where d is wire-to-wire distance.

lution pattern is shown in Fig. 6(a), while the resulting line spread function (LSF) is shown in Figs. 6(b). The Fermi function of the form $f(x)=a+b/[\exp(x-c)/d+l]$, where x is the distance, was fitted to the experimental ESF points and it shown as a solid curve in Fig. 6(a). Coefficient of determination (COD) is equal to 0.9746. The FWHM of the fitted Gaussian LSF is equal to 48.2 ± 0.5 μm with COD$=0.9978$. It is well known that the modulation transfer function (MTF) of a focal spot with a Gaussian intensity distribution is also a Gaussian function.[14,15] Therefore, we can easily predict MTF due to the focal spot for different object magnifications (M). Results obtained for a FWHM equal to 48 μm and M equal to 1.05, 1.5, 2, and 3, respectively, are shown in Fig. 7.

In Fig. 7 we have also included the predicted Gaussian MTF at $M=1.05$ produced by a hypothetical Gaussian source with FWHM$=500$ μm, which approximates a typical focal spot encountered in clinical mammography. We note that in reality the clinically observed focal spot MTF might be worse due to a nonsingle Gaussian brightness distribution.[14] We observe that the FWHM$=48$ μm at $M=2$ results in a MTF comparable to the MTF produced by a source with FWHM $=500$ μm (i.e., clinical focal spot) in the contact technique; see Fig. 7.

We have also imaged a Kodak mammographic phantom, see Fig. 5, for which we were able to resolve a 104 μm mesh pattern that is consistent with the estimated size of the focal spot.

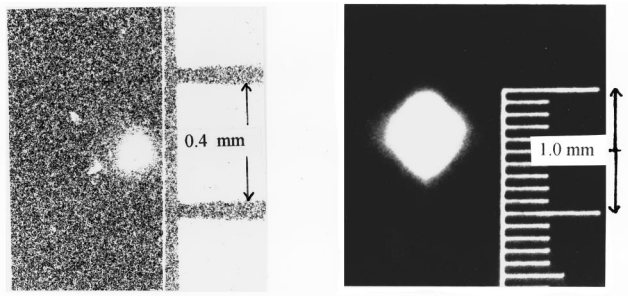

FIG. 4. An image of the x-ray focal spot created by laser produced plasma (left) and an image of the microfocal spot created by a dedicated clinical Mo mammography unit imaged using a pinhole camera (right). The arrow marks 0.4 and 1.0 mm distance for the left and right image, respectively.

III. DISCUSSION

In the following section we discuss the prospects of the LPP x-ray source for mammography.

A. The focal spot size

The imaging tasks of mammography include detection of small (below 100 μm) microcalcifications and visualization of structural characteristics of abnormal soft tissue masses. Therefore, it is obvious that a focal spot as small as possible must be used. In this study we have demonstrated that a focal spot size of the order of tens of micrometers can be realized by the LPP x-ray source. After monochromatization by a bent crystal monochromator the virtual focal spot size will be limited by the exit aperture and will be comparable to the LPP size. The availability of such a small focal spot would not only significantly improve resolution of present day contact mammography with antiscatter grids, but it might make magnification mammography (with $1.4<M<2$) practical. In this latter technique a spatial resolution exceeding 20 lp/mm can be achieved (see Fig. 7). Recently, we have shown that a large airgap (i.e., of the order of 40 cm or more) can be used as an antiscatter device equivalent to a mammographic antiscatter grid.[16] Therefore, in the proposed magnification mammography system, the need for an antiscatter grid would be eliminated. Consider a mammography system with the source-to-patient distance equal to 70 cm and a large airgap (40–70 cm). The expected average glandular dose (AGD) can be evaluated as follows: Let N_0 denote the fluence of photons on the detector needed to produce a desired contrast. For the contact technique with a grid the total number of

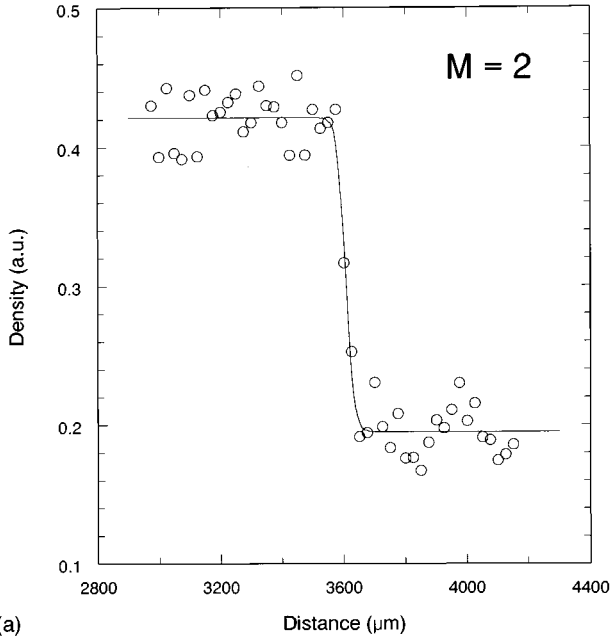

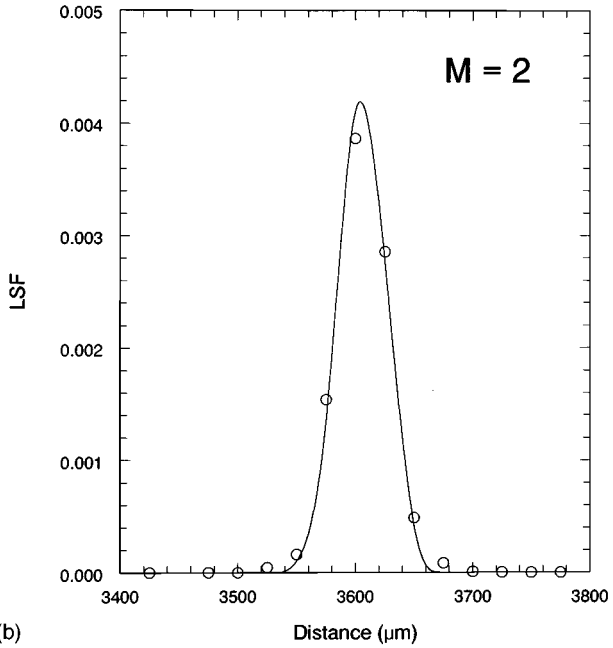

FIG. 6. (a) The edge spread function (ESF) inferred from the microdensitometer trace of the resolution pattern shown in Fig. 5 (open circles). The vertical axis is in arbitrary optical density units while the horizontal axis is the distance on film in units of μm. The Fermi function of the form $f(x)=a+b/[\exp(x-c)/d+l]$, where x is the distance on film, was fitted to the experimental points and is shown as a solid curve. The coefficient of determination (COD) is equal to 0.9746. (b) The line spread function obtained by differentiating the ESF-Fermi function from (a) is shown as open circles. The best fit assuming a Gaussian edge spread function is shown as a solid curve (FWHM=48.2±0.5 μm, COD = 0.9978).

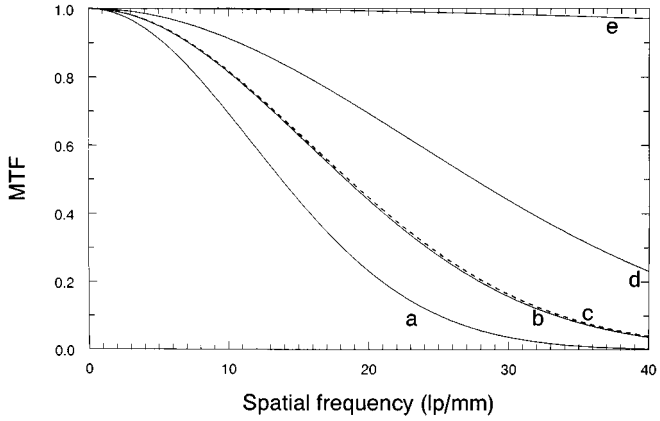

FIG. 7. Predicted modulation transfer functions (MTF) due to a focal spot with a single Gaussian brightness distribution for different object magnifications (M) and full width at half maximum (FWHM): (a) $M=3$, FWHM=48 μm; (b) $M=2$, FWHM=48 μm; (c) $M=1.05$, FWHM=500 μm; (d) $M=1.5$, FWHM=48 μm; (e) $M=1.05$, FWHM=48 μm.

polychromatic photons before a grid is therefore equal to BN_0 (where B is the Bucky factor). For the magnification technique in the quasimonochromatic mode the total number of photons before an airgap is equal to $\alpha M^2 N_0$ (where M is magnification and α is an energy- and tissue-dependent fluence reduction factor due to x-ray monochromatization). Accordingly, the expected exposure ratio for the two techniques can be evaluated as $\alpha \leqslant \alpha M^2 N_0 / B N_0 \leqslant 2\alpha$, for $1.4 < M < 2$ and an experimentally[16] obtained value of $B \approx 2$. We note that depending on energy and tissue characteristics, $0.5 \leqslant \alpha \leqslant 1$. Therefore, we conclude that the dose produced by the quasimonocohromatic LPP airgap system in the magnification mode ($1.4 < M < 2$) is comparable to the dose due to a standard Mo-based unit with a grid. A discussion of the average glandular dose in a conventional magnification mammography with a short airgap can be found in Ref. 17.

B. The x-ray beam quality

The spectral distributions of x radiation (i.e., the number of photons per energy interval versus photon energy) produced by a LPP x-ray source using a thick Mo target and a standard Mo x-ray tube, are shown in Fig. 8. Both sources utilized 30 μm of Mo as a filter. We notice the lack of a high cutoff point in the LPP x-ray spectrum. It should be emphasized that the undesired high-energy tail in the LPP spectral distribution can be significantly reduced by the utilization of a thin target if its thickness does not exceed the 25 keV electron range in the target material. The low-energy tail in the spectrum (10–15 keV) would be almost entirely absorbed by the breast tissue, thus resulting in increased AGD without any benefit to the image quality, and should be eliminated as well. Clearly, in an ideal mammography system the beam quality should be tailored to the parameters of a specific patient. A useful figure of merit, which should be optimized, is the signal-to-noise ratio per unit of absorbed dose versus mean energy and the bandwidth of x rays. The energy at which this parameter reaches a maximum depends strongly on the compressed breast tissue thickness and to a lesser degree on the breast tissue composition, image detector characteristics and some other factors. The calculated optimum mean x-ray energies are in the range of 15–18 keV and 21.5–25 keV for a 2.5 and 8 cm thick breast,

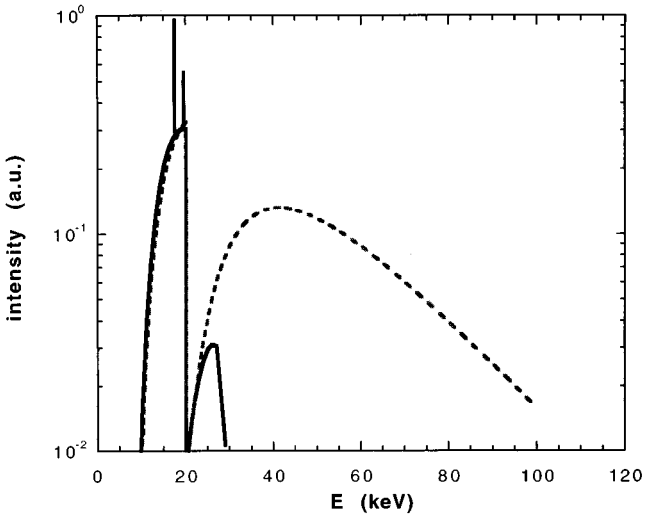

FIG. 8. The spectral distribution of x-rays produced by a LPP x-ray source (dashed curve) versus a standard Mo x-ray tube (solid curve) obtained for a thick Mo target. The ordinate is number of x-ray photons per energy interval normalized to emission at the K_α line. Both spectra were obtained with 30 μm of Mo filtration.

respectively.[17–22] It can be shown that if polychromatic radiation with a fixed photon energy distribution is used, such as that produced by a standard Mo x-ray tube, the photon fluence that is in the optimum band for a given breast thickness decreases dramatically for thicker breasts; e.g., for the Mo/0.03 mm Mo system, it decreases from 57% to 6% for 2.5 and 8 cm breast thicknesses, respectively.

For a laser-driven x-ray source the beam quality optimization can be best accomplished by the utilization of a spherically bent, high luminosity, crystal monochromator in a fixed-exit Rowland circle configuration.[23–25] This tunable device utilizes the phenomenon of Bragg reflection from spatially periodic structures, such as crystals, to filter out a spectrally narrow band (0.02–1 keV) of x rays. As a result, a cone beam emanating from a spatially fixed virtual focal spot, formed by the monochromator exit aperture, can be created (see Fig. 9). We note that the LPP x-ray source (i.e., the focal spot of the laser), the center of the bent crystal, and the exit aperture lay on the Rowland circle. The mean energy of the beam can be precisely adjusted to a specific patient, thus resulting in the lowest possible exposure for the highest possible subject contrast for a given breast thickness and composition. The comparison of AGD due to the usage of a tunable quasimonochromatic x-ray source over a standard Mo tube is given in Table I. We observe that the advantage in terms of AGD becomes significant ($\sim$40%) for breast thicknesses over 4 cm. We note that 4 cm the average compressed breast thickness. The increased signal-to-noise ratio achieved with a spectrally narrow beam certainly would improve the sensitivity of a mammographic examination for any breast thickness due to the elimination of the beam hardening effect.

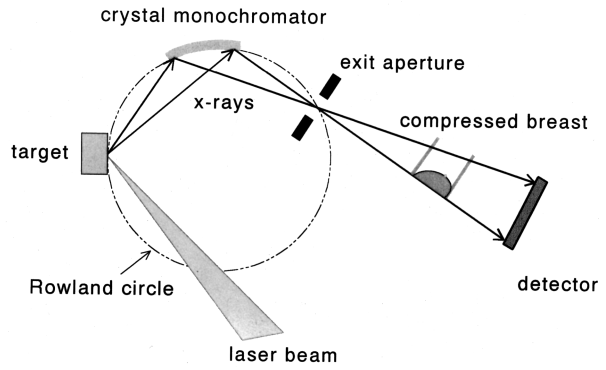

FIG. 9. A design of a laser-based mammography unit with spherically bent crystal monochromator and a large airgap as an antiscatter device. The target, bent crystal monochromator and focus of quasimonochromatic x rays are located on the Rowland circle with a 1 m radius.

TABLE I. Comparison of the average glandular dose (AGD) received using LPP quasimonoenergetic versus Mo/(0.03 mm Mo) polyenergetic x-ray source. $25kV_P$ was used for a Mo system with the exception of breast thickness $d = 8$ cm, for which $28kV_P$ was used. The optimum monochromatic energy for a specific breast thickness was selected (Refs. 18–22). For simplicity the energy- and tissue-dependent fluence reduction factor α due to x-ray monochromatization was assumed to be equal to 1 ($\alpha = 1$) for all energies, which results in overestimation in AGD due to quasimonoenergetic x rays. Therefore, since the $0.5 < \alpha < 1$, the values listed in the third column of the table should be regarded as the upper limit.

X-ray energy (keV)	Thickness (cm)	AGD using LPP source with a monochromator (millirad)[a]	AGD using Mo anode and Mo filter (millirad)[b]
16	2	65	50
19	4	100	120
21	6	180	450
23	8	270	425

[a]Dose calculated assuming 50% glandular/50% adipose breast composition.
[b]Dose measured using a 50% glandular/50% adipose phantom.

C. Minimum laser pulse energy required and overall power consumption

We assume that an initial exposure of the order of 300 mR per image is required in mammography performed with monoenergetic radiation, which corresponds to 1.8×10^9 photons/cm^2 of monoenergetic x-ray photons with 20 keV energy.[26] Therefore, the LPP x-ray source has to create an x-ray fluence of at least 1.8×10^9 photons/cm^2 in the narrow band ($\Delta E\cong1$ keV) in the spectral range 15–25 keV. For the narrow band of x rays with $h\nu=20$ keV, the equivalent energy fluence is $6\,\mu$J/cm^2. If the FOV is 18×24 cm^2 = 432 cm^2 then

$$E_{\text{x rays}}=\Phi_{\text{x rays}}\times\text{area}$$

$$=6\times10^{-6}\ \text{J/cm}^2\times432\ \text{cm}^2=2.6\times10^{-3}\ \text{J}. \qquad (1)$$

The efficiency f_m of the photon collection and monochromatization system can be evaluated as follows: The solid angle intercepted by a bent crystal with an effective area 25 $\times$ 25 cm^2, with the source approximately 100 cm away, is

$$\Delta\Omega=25\times25\ \text{cm}^2/100^2\ \text{cm}^2=62.5\times10^{-3}. \qquad (2)$$

The Bragg reflection efficiency is of the order of $f_B = 30\%$, in the 15–25 keV regime, therefore

$$f_m = f_B \times \Delta\Omega/2\pi = 0.3 \times 62.5 \times 10^{-3}/2\pi = 3 \times 10^{-3}, \quad (3)$$

and assuming conversion efficiency $f_x = 2 \times 10^{-4}$, the required laser pulse energy is 4.3 kJ [see Eq. (4)],

$$E_{\text{laser}} = E_{\text{x rays}}/(f_m \cdot f_x) = 2.6 \times 10^{-3} \text{ J}/(3 \times 10^{-3} \cdot 2 \times 10^{-4}) = 4.3 \text{ kJ}. \quad (4)$$

The desired photon fluence can be generated in a single laser pulse using a high-energy laser or a train of short pulses produced by a high repetition rate TTT laser.[27] Since the quasimonochromatic x-ray flux is approximately proportional to the beam spectral width, the available flux can be increased in proportion to the monochromator spectral width ΔE. That is, if the increase in ΔE from 1 keV to N keV is acceptable then the required laser pulse energy can be lowered by a factor of N.

High-power and high repetition rate lasers are not very efficient sources of light and presently (depending on the laser type) only 1%–10% of the power drawn form the plug in the wall is converted to coherent laser radiation. Therefore, they might consume as much as 300 kW of power and require complex methods of heat removal. In this aspect they resemble high-power x-ray tubes.

D. Target design

In the LPP source, x rays are generated by the interaction of a high-power laser beam with a solid target. This method differs in a number of ways from the use of a traditional, electron-beam x-ray source. In the rotating anode, the heat load must be restricted because the anode is reused. Thus, the temperature of the anode must be kept below the melting temperature (actually below the recrystallization temperature). In the laser x-ray source, a fresh target material is used on every shot. The surface of the target where the laser beam was focused is ablated and subsequently ionized. As a result a shallow ($\sim 100\ \mu$m) ''crater'' is created. A number of techniques are commonly used to provide a new target surface on every shot. The target can either be a rotating disk,[1] a rastered plane, a target ''tape,'' or a ''self-healing'' target in a form of liquid metal. In the three former cases, the target is moved one step between each shot so that a fresh surface is exposed at every shot. The step size is determined by the size of the crater created by the laser interaction and the target cleanliness requirements. For high repetition rate work a computerized target positioning system utilizing an alignment laser in an optical feedback loop will be necessary in order to minimize the effective focal spot size. The target positioning requirements are determined by the requirements of the monochromator geometry and condition that the target is located within one Rayleigh range of the focus.

E. Cost and size estimates for laser systems for mammography

The laser system required for quasimonochromatic x-ray mammography will need to operate at ~ 0.1 Hz with a pulse energy of ~ 1 kJ or at 1 kHz with a pulse energy of ~ 1 J. The former laser systems with similar parameters are currently commercially available.[28] These laser systems are either pulsed solid state systems using Nd-doped materials or pulsed gas discharge systems using CO_2. As an example of the cost of such a laser system, Lumonics, Inc. sells a 0.4–2.5 kW average power pulsed industrial system for \$70 000–\$120 000. These include both solid state and CO_2 laser systems. The high repetition laser systems are currently a subject of research and are not commercially available, therefore at this time it is difficult to estimate their price. The cost of the monochromator and target system should not exceed \$200 000. Thus, one would expect that the whole LPP-based narrow band mammography system should cost $\sim$\$350 000.

We expect that physically the whole system can be placed in a standard x-ray suite.

IV. CONCLUSIONS

We have created a laser-produced plasma (LPP) x-ray source with a very small focal spot, two-dimensional Gaussian brightness distribution (FWHM$\approx 50\ \mu$m), very short duration (~ 4 ps), and spectral distribution that might be suitable for mammography. We have shown that the LPP source in conjunction with a spherically bent, high throughput, crystal monochromator in a fixed-exit Rowland circle configuration, can be used to construct a narrow band and tunable mammography system. The LPP x-ray source could also be used in conjunction with the existing contact mammography grid systems. The tunability to a given patient breast tissue thickness and density would allow one to significantly improve contrast and resolution (exceeding 20 lp/mm) while lowering the exposure up to 50% for thicker breasts (see Table II). The LPP source might make it feasible to create a mammography unit that could work in a magnification mode ($1.4 \leqslant M \leqslant 2$) with a large airgap used as an antiscatter device instead of a grid (see Fig. 9). The radiation dose delivered by this device would be still comparable to the dose delivered by a grid mammography system.

ACKNOWLEDGMENT

This work was supported in part by NIH/NHLBI Grant No. R01 HL52643-01A2.

[1] K. Herrlin, G. Svahn, C. Olsson, H. Petterson, C. Tillman, A. Persson, C. G. Wahlström, and S. Svanberg, ''Generation of x rays for medical imaging by high-power lasers: Preliminary results,'' Radiology **189**, 65–68 (1993).

[2] J. C. Kieffer, P. Audebert, M. Chaker, J. P. Matte, H. Pepin, X. Johnston, P. Maine, D. Meyerhofer, J. Delettrez, D. Strickland, P. Bado, and G. Mourou, ''Short pulse laser absorption in very steep plasma density gradients,'' Phys. Rev. Lett. **62**, 760–763 (1989).

[3]J. C. Kieffer, M. Chaker, J. P. Matte. C. Y. Cote, Y. Beaudoin, Z. Jiang, C. Y. Chien, S. Coe, G. Mourou, O. Peyrusse, and D. Gilles, ''Ultrafast x-ray emission from ultrashort plasmas,'' SPIE Proc. **1860**, 127–132 (1993).
[4]X. B. Liu and D. Umstadter, ''Competition between ponderomotive and thermal forces in short scale length laser plasmas,'' Phys. Rev. Lett **69**, 1664 (1992).
[5]J. C. Kieffer, Z. Jiang, A.Ikhlef, C. Y. Cote, and O. Peyrusse, ''Picosecond dynamics of a hot solid density plasma,'' J. Opt. Soc. Am. B **13**, 132–137 (1996).
[6]C. Joshi and P. B. Corkum, ''Interactions of ultra-intense laser light with matter,'' Phys. Today **48**, 36–43 (1995).
[7]W. Kruer, *The Physics of Laser Plasma Interaction*, edited by D. Pines (Addison-Wesley, Reading, MA, 1987), p. 153.
[8]J. D. Kmetec, C. L. Gordon, III, J. J. Macklin, B. E. Lemoff, G. S. Brown, and S. E. Harris, ''MeV x-ray generation with femtosecond laser,'' Phys. Rev. Lett **68**, 1527–1530 (1992).
[9]A. Fews, P. Norreys, F. Gbeg, A. Bell, A. Dangor, C. Danson, P. Lee, and S. Rose, ''Plasma ion emission from high intensity picosecond laser pulse interactions with solid targets,'' Phys. Rev. Lett **73**, 1801 (1994).
[10]W. R. Hendee, *Medical Radiation Physics* (Year Book Medical Publishers, Chicago, 1970), p. 73.
[11]H. Pein, F. Martin, B. Grek, T. W. Johnson, J. C. Kieffer, and G. Mitchel, ''Evidence of pondermotive processes from x-ray spectra of CO_2 laser-irradiated targets,'' J. Appl. Phys. **50**, 6784–6788 (1979).
[12]Z. Jiang, J. C. Kieffer, J. P. Matte, M. Chaker, A. Ikhlef, O. Peyrusse, D. Gilles, G. Korn, A. Maksimchuk, S. Coe, and G. Mourou, ''X-ray spefctroscopy of hot solid density plasmas produced by subpicosecond high contrast laser pulses at 10^{18}–10^{19} W/cm^2,'' Phys. Plasmas **2**, 1702–1711 (1995).
[13]E. L. Nickloff, E. Donnelly, L. Eve, J. V. Atherton, and T. Asch, ''Mammographic resolution: Influence of focal spot intensity distribution and geometry,'' Med. Phys. **17**, 436–447 (1990).
[14]A. P. Tzannnes and J. M. Mooney, ''Measurements of the modulation transfer function of infrared cameras,'' Opt. Eng. **34**, 1808–1817 (1995).
[15]S. C. Prasad, W. R. Hendee, and P. L. Carson, ''Intensity distribution, modulation transfer function, and the effective dimension of a line-focus x-ray focal spot,'' Med. Phys. **3**, 217–223 (1976).
[16]A. Krol, D. A. Bassano, C. C. Chamberlain, and S. C. Prasad, ''Scatter reduction in mammography with air-gap,'' Med. Phys. **23**, 1263–1270 (1996).
[17]B. Liu, M. Goodsitt, and H. P. Chan, ''Normalized average glandular dose in magnification mammography,'' Radiology **197**, 27–32 (1995).
[18]J. W. Motz and M. Danos, Med. Phys. **5**, 8–22 (1975); E. P. Muntz, M. Welkowski, E. Kaegi, L. Morsell, E. Wilkinson, and G. Jacobson, Radiology **127**, 517–523 (1978).
[19]R. J. Jennings and T. R. Fewell, in *Reduced Dose Mammography*, edited by W. W. Logan and E. P. Munty (Masson, New York 1979), pp. 211–222; D. Dance and G. Day, in *Proceedings of the Seminar on Patient Exposure in Medical X-ray Diagnosis*, Munich, Germany, EUR. 7438 (Commission of European Community, Brussels, 1981), pp. 227–244.
[20]R. J. Jennings, R. J. Eastgate, M. P. Siedband, and D. L. Ergun, ''Optimal spectra for screen-film mammography,'' Med. Phys. **8**, 629–639 (1981); S. A. Beaman and S. C. Lillicrap, ''Optimum x-ray spectra for mammography,'' Phys. Med. Biol. **27**, 1209–1220 (1982).
[21]C. P. MacDonagh, J. L. Leake, and S. A. Beaman, ''Optimum x-ray spectra for mammography: Choice of K-edge filters for tungsten anode tubes,'' Phys. Med. Biol. **29**, 249–252 (1984).
[22]R. E. Johnston, D. W. Washburn, E. Pisano, C. Burns, W. C. Thomlinson, L. D. Chapman, F. Afrelli, N. F. Gmur, Z. Zong, and D. Sayers, ''Mammographic phantom studies with synchrotron radiation,'' Radiology **200**, 659–663 (1996).
[23]M. Lemmonier, R. Fourme, R. Roueaux, and R. Khan, ''X-ray curved-crystal monochromator system at the storage ring DCI,'' Nucl. Instrum. Methods **152**, 173–177 (1978).
[24]P. Platz, J. Ramette, E. Bellin, C. Bonnele, and A. Gabriel, ''High-throughput, high-resolution soft x-ray crystal spectrometer for tokamak-plasma studies,'' J. Phys. **14**, 448–452 (1981).
[25]W. Thulke, R. Haensel, and P. Rabe, ''Versatile curved crystal spectrometer for laboratory EXAFS measurements,'' Rev. Sci. Instrum. **54**, 277–283 (1983); A. V. Rode, A. M. Maksimuchuk, G. V. Sklizov, A. Ridgeley, C. Danson, N. Rizivi, R. Bann, E. Forster, and I. Uschmann, ''Intensity measurements of a quasi-monochromatic x-ray beam formed by a spherically bent crystals,'' Opt. Commun. **27**, 163–166 (1990).
[26]H. E. Johns and J. R. Cunningham, *The Physics of Radiology* (Thomas, Springfield, IL, 1983), Chap. 8.
[27]M. Perry and G. Mourou, ''Terawatt to petawatt sub-picosecond lasers,'' Science **264**, 917–924 (1994).
[28]See, for example, the Laser Focus World Buyers Guide, 1996.